Aerospace Science and Technology 154 (2024) 109532

Contents lists available at ScienceDirect

Aerospace Science and Technology

journal homepage: www.elsevier.com/locate/aescte

Surrogate based design space exploration and exploitation for an efficient airfoil optimization under uncertainties using transition models

Jigar Parekh [a,b,*], Philipp Bekemeyer [a,b], Sebastian Helm [a,b], Daniela Gisele François [b], Cornelia Grabe [a,b]

[a] Cluster of Excellence SE²A – Sustainable and Energy-Efficient Aviation, TU Braunschweig, Braunschweig, Germany
[b] Institute of Aerodynamics and Flow Technology, German Aerospace Center (DLR), Braunschweig/Göttingen, Germany

ARTICLE INFO

Communicated by Jérôme Morio

MSC:
0000
1111

Keywords:
Robust design optimization
Surrogate based uncertainty quantification
Design exploration and exploitation
Laminarization
Transition modeling

ABSTRACT

The pursuit of sustainable, zero-emission air travel is heavily dependent on the creation of energy-efficient aircraft. Key strategies for achieving this sustainability in aviation include reducing fuel consumption through low-drag designs harnessing laminar flow. However, designing aircraft with laminar flow characteristics is complex due to their sensitivity to environmental and operational factors. This study tackles the challenge of developing energy-efficient aircraft by using computational fluid dynamics models and sophisticated optimization techniques that account for uncertainty. Our approach demonstrates the effectiveness of surrogate-based optimization and uncertainty quantification in optimizing airfoil drag for a natural laminar airfoil (NLF) design. We use surrogate models, trained with data from detailed airfoil simulations, which include a boundary layer code coupled with a linear stability method and a newly developed transition transport model. Transition location predicted using transition models facilitate an accurate drag prediction used in the optimization process. The accuracy of these surrogate models is enhanced through active sampling strategies. Our robust optimization method considers uncertainties in environmental and operational conditions, offering a deeper insight into their effects on crucial design parameters. Unlike traditional deterministic aerodynamic design optimization, our findings highlight the efficacy and precision of uncertainty-based optimization in achieving robust NLF airfoil designs over large (exploration mode) and small (exploitation mode) design spaces. Investigating design space parameterization based on the size of design variables reveals significant differences in optimal airfoil configurations. The optimized designs we propose favor delayed transition, in contrast to deterministic designs which often result in significant loss of laminarity when facing uncertainties. This study represents a significant advancement in aerospace engineering, providing a practical and effective methodology for creating energy-efficient airfoil designs. The application of these advanced optimization and uncertainty quantification techniques shows great potential for the wider field of aerospace engineering, paving the way for more resilient and robust aircraft designs.

1. Introduction

An ongoing challenge in commercial aviation is to reduce fuel consumption, driven by the need to meet stringent environmental targets set by aviation regulatory bodies. The European Commission, for example, has outlined goals of reducing CO_2 emissions by 75% and NO_x emissions by 90% per passenger kilometer by 2050 [1]. This effort not only addresses environmental concerns but also aims to reduce operational costs for airlines. Through the evolution of aviation, advances in aircraft design have led to more efficient commercial aircraft. However, as the fundamental 'tube and wing' design of aircraft has largely remained unchanged, each new design iteration offers only incremental improvements in efficiency. To make significant progress in aircraft performance, it's crucial to explore new aerodynamic configurations and leverage more complex airflow phenomena.

One such approach is the passive extension of laminar flow, known as Natural Laminar Flow (NLF), which extends the laminar boundary layer, reducing viscous drag and thereby improving aerodynamic efficiency [2]. Achieving NLF involves suppressing boundary-layer instabilities that cause flow transition. NLF benefits have so far been pri-

* Corresponding author.
E-mail address: jigar.parekh@dlr.de (J. Parekh).

https://doi.org/10.1016/j.ast.2024.109532
Received 11 April 2024; Received in revised form 23 August 2024; Accepted 26 August 2024
Available online 30 August 2024

marily explored for low swept wings at lower Reynolds numbers where boundary-layer instabilities are minimal [3]. At higher Reynolds numbers and sweep angles, crossflow instabilities near the leading edge can lead to turbulent flow [4]. However, by designing specific pressure profiles, it is possible to counteract these instabilities without active flow control devices [5]. Traditional NLF airfoil design achieves this through careful manipulation of pressure distribution [6,7].

Designing laminar wings typically involves inverse design methods based on linear stability theory (LST) [6,8], aiming to maintain laminar flow by specifying desired pressure distributions. While effective, these methods may not always yield optimal designs and heavily depend on the experience of the engineer. An emerging alternative is direct optimization methods, which offer a broader exploration of the design space and can often produce better results than inverse design approaches. Aerodynamic shape optimization is well-established in both academia and industry [9]. For instance, direct shape optimization has been employed in designing NLF airfoils and wings [10]. Previous studies have designed NLF airfoils across various Mach numbers and lift coefficients to achieve robust configurations [11], focusing on minimizing a combination of the mean and standard deviation of the drag coefficient.

To design and analyze laminar flow wings, it is essential to have transition prediction and modeling techniques that can accurately capture all relevant transition mechanisms. These methods should also consider the effects of surface irregularities like roughness and surface waviness, as well as the impact of surface suction. The e^N method is widely used in industry for transition prediction [12] and considered here as reference method. The more recent DLR γ model [13] which offers advantages in terms of automation and ease-of-use is considered to evaluate its applicability in the design process. The critical N-factors in e^N method are an integral measure of the flow quality and are strongly depending on disturbances, such as freestream turbulence intensity, surface imperfections and noise, and boundary-layer receptivity to these disturbances. The environmental uncertainties can be expressed as uncertainties in these critical N-factors. Similarly, environmental uncertainty can be expressed in terms of variation in the freestream turbulent intensity when the DLR γ model is used. Moreover, the variability in the flight conditions can not be neglected and must be considered as operational uncertainties in the design process. Therefore, using the above-mentioned high-fidelity methods for an effective implementation of NLF becomes complex due to sensitivity to the uncertain environmental as well as operational conditions [14].

There is a notable gap in real-world applications of robust design methodologies for NLF, particularly in scenarios involving swept wings. Previous efforts have largely relied on low-fidelity simulations focusing on 2D instabilities, limiting their applicability to more complex scenarios. Robust design optimization under uncertain critical N-factors has been proposed [15], using tools like XFOIL combined with boundary-layer solvers and the e^N transition model. More recently, an efficient bilevel approach for optimization under uncertainty has been proposed [16], where the authors considered the uncertainty not only in the N-factors but also in the operational conditions. While environmental uncertainties have been explored for the e^N method, similar analysis for transition transport models like the DLR γ model is still lacking. A robust optimization using Reynolds-averaged Navier–Stokes (RANS) simulations with both the e^N method and the DLR γ model, presents an opportunity for such a comprehensive analysis. Moreover, most of the literature focuses on a relatively limited design space, primarily centered around baseline configurations resulting into a sub-optimal design owning to feasible-yet-unexplored design space. A surrogate based design optimization framework can facilitate exploration of a larger design space at a considerably lower computational cost compared to other global optimization techniques.

This study focuses on three primary objectives: (i) utilizing a probabilistic framework [17] for designing robust NLF transonic airfoils that are resilient against uncertain environmental and operational conditions at high sweep and Reynolds numbers, (ii) comparing the robust (and deterministic) optimum designs obtained using both the e^N method and DLR γ model, and (iii) comparing the optimum designs resulting from larger and smaller design spaces, regarded as exploration and exploitation mode design spaces, respectively.

The paper is structured as follows: Section 2 introduces the bilevel robust optimization framework using surrogate models. Section 3 details the setup for transonic airfoil optimization under uncertainty, including problem formulation, flight conditions, transition models, environmental uncertainties, design space parameterization, and the numerical model for computing aerodynamic quantities of interest (QoIs). Section 4 presents the results from deterministic and robust optimization using both transition models and exploration as well as exploitation mode. Finally, conclusions are offered in section 5.

2. Methodology

Addressing a global optimization issue might necessitate numerous evaluations of a function (regarded as a black-box) which varies with the complexity of the design space and non-linearity of the function. This process can quickly become unmanageable and impractical, particularly when the design space is multi-dimensional or the function evaluation is costly (like a standard CFD simulation). Additionally, the computational burden increases significantly due to the need for a statistical evaluation at each step as explained in the following section. To address these challenges, an effective surrogate-based robust optimization approach is employed, which has been demonstrated successfully in [17].

2.1. Optimization problem

Let $Y \in \mathbb{R}$ be the quantity of interest (QoI) which is usually a performance measure such as drag coefficient, depending (typically nonlinearly) on the design variables $\boldsymbol{x} \in \mathbb{R}^d$ at operating conditions $\boldsymbol{A}$. The goal of *deterministic* optimization is to find an optimal set of design variables $\boldsymbol{x}^*$ at constant (nominal) operating conditions $\boldsymbol{A}_0$ while satisfying k constraints on the design variables,

$$\begin{aligned} &\boldsymbol{x}^* = \underset{x}{\operatorname{argmin}}\{Y(\boldsymbol{x}, \boldsymbol{A}_0)\}, \\ &g_i(\boldsymbol{x}) \leq 0, \quad i = 1, 2, ..., k. \end{aligned} \tag{1}$$

Robust optimization focuses on identifying an optimal design while accounting for uncertainties in environmental and/or operational conditions, represented as $\boldsymbol{\xi} \in \mathbb{R}^m$. As a result, the QoI is treated as a random variable. This alters the optimization objective from simply optimizing the QoI to optimizing a significant statistic of the QoI. To achieve this, the statistic of the QoI, such as the mean, standard deviation, or quantile, is calculated using uncertainty propagation methods. The optimizer then aims to minimize this statistic. In this study, the mean value of the QoI, denoted as μ_Y, is considered, and the robust optimization problem is defined accordingly.

$$\begin{aligned} &\boldsymbol{x}^* = \underset{x}{\operatorname{argmin}}\{\mu_Y(\boldsymbol{x}, \boldsymbol{\xi})\}, \\ &g_i(\boldsymbol{x}) \leq 0, \quad i = 1, 2, ..., k. \end{aligned} \tag{2}$$

Note that, choosing standard deviation as the objective function of the optimization process may provide an airfoil which is less sensitive to the uncertainties but may not guarantee an improved mean performance over the baseline airfoil. Ultimately the choice of the objective functions depends on the user and their application at hand. The methodology as such remains unchanged from alterations in objective function.

2.2. Surrogate-based approach for robust optimization

A versatile bilevel surrogate model framework has been effectively applied to a variety of robust design optimization challenges with a moderate level of dimensions and uncertainties, as referenced in [17,16].

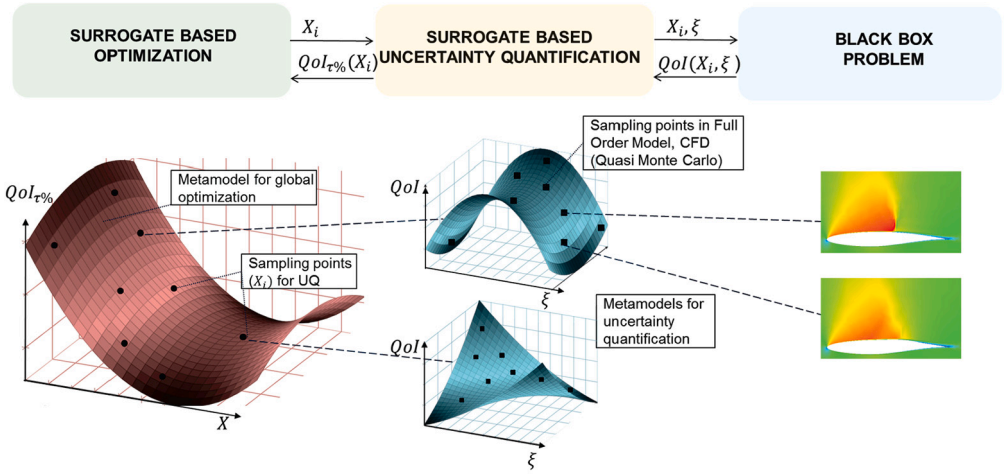

Fig. 1. Bilevel approach for robust optimization [17]: surrogate of statistics (left), surrogate of random variable (middle), and full-order model evaluation (right). (For interpretation of the colors in the figure(s), the reader is referred to the web version of this article.)

This framework, depicted in Fig. 1, integrates two loops: an outer loop using a Surrogate-Based Optimization (SBO) approach, and an inner loop employing a Surrogate-Based Uncertainty Quantification (SBUQ) method. In each optimization cycle, only the design variables $\boldsymbol{x}$ are entered into the SBO surrogate (illustrated by the red response surface), producing the QoI's statistic as output. Conversely, the SBUQ surrogate (shown as the blue response surface) takes the uncertainties $\boldsymbol{\xi}$ as input for a set of (fixed) design variables and outputs the QoI, calculated via a black-box function.

This gradient-free robust optimization framework is particularly beneficial for CFD simulations that involve transition predictions using the e^N method or the DLR γ model, which do not yield adjoint solutions in a straightforward manner. The framework's overall efficiency is further boosted by refining the area around the optimal solution through infill (adaptive sampling) techniques. Additionally, the efficiency is enhanced by the parallel evaluation of the design of experiments (DoE) and the inherent parallelization capabilities of the black-box CFD solver.

2.2.1. Optimization

The primary aim of the outer loop (SBO) in the bilevel framework is to conduct an efficient optimization using a minimal number of costly black-box evaluations, as noted in [18]. To achieve this, a surrogate model is constructed that not only links the design variables to the QoI but is also economical to evaluate.

The SBO module of the Surrogate-Modelling for AeRo-data Toolbox in pYthon (SMARTy), developed by the German Aerospace Center (DLR), is utilized in this process, as referenced in [19]. This optimization module (i) initiates the design space exploration with a DoE sampling and evaluating the objective function (and constraints), (ii) constructs a surrogate model for the objective function (and constraints), (iii) applies an active infill criterion to progressively identify the optimum, requiring black-box solver evaluations for each proposed optimal design, and (iv) updates the surrogate model(s) after each infill iteration. For the DoE phase, Sobol sequence is employed [20], and for surrogate modeling, Kriging (Gaussian process regression) models are used [21]. Further details on constructing a Kriging model are available in Appendix A.

The infill criterion implemented in this study is the *expected improvement* (EI) method. This method is based on the normal distribution predictions (mean $\hat{y}(\boldsymbol{x})$ and standard deviation $\hat{\sigma}(\boldsymbol{x})$) of the objective function derived from the Kriging surrogate at any specific point $\boldsymbol{x}$ in the design space, as outlined in [22]. The EI is calculated using the likelihood of improvement compared to the current best sampled solution y_{min}.

$$EI[(\boldsymbol{x})] = \left(y_{min} - \hat{y}(\boldsymbol{x})\right) \Phi\left(\frac{y_{min} - \hat{y}(\boldsymbol{x})}{\hat{\sigma}(\boldsymbol{x})}\right) + \hat{\sigma}(\boldsymbol{x}) \phi\left(\frac{y_{min} - \hat{y}(\boldsymbol{x})}{\hat{\sigma}(\boldsymbol{x})}\right), \quad (3)$$

where Φ and ϕ are the cumulative and probability distribution functions of the standard normal distribution, respectively. The EI infill method balances exploration with exploitation in the sense that a large expected improvement is present in the regions where a solution smaller than the current best is possible and/or in the regions where the model error is large. The EI implementation in SMARTy accounts for the probability of feasibility by computing the probability of not violating the constraints and multiplying it to the EI value at a given location. Differential evolution is employed to locate the optimal position where EI is maximum. The refining continues until the convergence criteria (L2 distance between consecutive design vectors or the EI values) or the maximum number of infill points (budget) is reached.

2.2.2. Uncertainty quantification

The objective of the inner loop (SBUQ) in the bilevel framework is to effectively propagate the input uncertainties to the QoI, and then to precisely estimate the QoI's statistical measures for use in SBO. To compute the statistics, instead of applying the Monte Carlo method in a conventional manner i.e. directly evaluating complex and expensive black box function, it is used to evaluate a simpler and inexpensive surrogate model, which represents the original function's behavior. This involves constructing a Kriging surrogate model based on the initial DoE conducted in the stochastic space, along with its evaluations (black-box solutions). This model maps the uncertainties to the QoI. To enhance the surrogate's accuracy, an active infill criterion based on statistics is utilized. In this case, the infill criterion focuses on the mean of the QoI, demanding high global accuracy of the surrogate.

The infill criterion employs the prediction mean square error $\hat{s}(\boldsymbol{\xi})$ at any given point $\boldsymbol{\xi}$ within the Kriging surrogate to ensure balanced sampling in the stochastic space. New samples are sequentially added—post updating the surrogate—at the location $\boldsymbol{\xi}^*$ where the product of the joint probability distribution function of the input uncertainties $\text{PDF}_{\boldsymbol{\xi}}$ and the error estimate is maximized. The minimization problem is thus formulated as:

$$\boldsymbol{\xi}^* = \underset{\boldsymbol{\xi}}{\text{argmin}} \{ -\text{PDF}_{\boldsymbol{\xi}}(\boldsymbol{\xi})\, \hat{s}(\boldsymbol{\xi}) \} \quad (4)$$

In this formulation, the $\text{PDF}_{\boldsymbol{\xi}}$ component prioritizes sampling from areas with higher probability in the stochastic space, while the error term $\hat{s}(\boldsymbol{\xi})$ targets regions where the surrogate model's accuracy is lower. Differential evolution is employed to locate the optimal position in the surrogate. The statistic of the QoI is then acquired using a large number of Quasi Monte Carlo samples evaluated using the surrogate model. The sampling choice is based on its efficiency and accuracy in high-dimensional

integration tasks, better convergence rates than traditional Monte Carlo methods, and its straightforward implementation.

3. Numerical setup

This section outlines the formulation of both deterministic and robust transonic airfoil optimization. It includes a detailed characterization of the design space and the uncertainties involved, as well as a description of the numerical model employed as the black-box solver.

3.1. Flight conditions

The deterministic and robust optimization processes aim to identify the optimal design for a transonic airfoil operating under specific conditions: Mach number 0.78, lift coefficient 0.7, Reynolds number 23×10^6, and a sweep angle of 27^o. At these conditions, attachment line transition, Tollmien-Schlichting transition and crossflow transition are the most relevant mechanisms leading to laminar-turbulent transition of the flow over aircraft wings. An analysis of flight test data of the Fokker 100 and the Advanced Technologies Testing Aircraft System (ATTAS) is presented in [23,24]. Attachment line transition can be prevented, for example using anti-contamination devices or Gaster bumps and is thus not considered in this study. In contrast to that, crossflow instabilities can be mitigated through careful wing profiling that reduces streamwise pressure gradients. On the other hand, larger streamwise pressure gradients are desirable to mitigate TS transition. This balance between different transition mechanisms can be effectively achieved through numerical optimization, facilitating extended regions of laminar flow even at higher Reynolds numbers and sweep angles.

3.2. Deterministic and robust optimization

In the present study, the deterministic optimization solves for the optimum design $\boldsymbol{x}^*$ that minimizes the drag coefficient at a constant (nominal) value of Mach number and lift coefficient. The maximum airfoil thickness normalized by chord length t/c_{max} is set to be greater than $t/c_{max,0} = 0.11$:

$$\begin{aligned} \boldsymbol{x}^* &= \underset{x}{\operatorname{argmin}}\{C_D(\boldsymbol{x}, M, C_L)\} \\ \text{s.t.} \quad & t/c_{max} \geq t/c_{max,0} \end{aligned} \tag{5}$$

The chosen maximum thickness-to-chord ratio ensures a balance between aerodynamic performance and structural integrity, thereby resulting in a reasonable trade-off between minimizing drag and maintaining sufficient structural strength and fuel volume.

The constant lift coefficient is handled by the CFD solver by iteratively adjusting the angle of attack. The maximum thickness constraint is set as a constraint in the optimization process.

In order to approximate realistic flight conditions, the robust optimization incorporates both environmental and operational uncertainties $\boldsymbol{\xi}$. As discussed earlier, the QoI (C_D) becomes a random variable, the statistic of which is therefore optimized. In order to obtain an overall good performance, in this study, the minimization of the mean values of the drag coefficient μ_{C_D} is sought.

$$\begin{aligned} \boldsymbol{x}^* &= \underset{x}{\operatorname{argmin}}\{\mu_{C_D}(\boldsymbol{x}, \boldsymbol{\xi})\} \\ \text{s.t.} \quad & t/c_{max} \geq t/c_{max,0} \end{aligned} \tag{6}$$

3.3. Design parameterization - exploration vs exploitation

In both deterministic and robust optimization, the objective function is influenced by the design variables $\boldsymbol{x}$, which determine the airfoil's shape. This study employs class shape function transformations (CSTs) to model and modify the airfoil's profile throughout the optimization iterations, as outlined in [25]. The CST parameterization describes a two-dimensional geometry using a combination of a class function $C(x/c)$, a shape function $S(x/c)$ based on Bernstein binomials, and an additional term for the trailing edge thickness:

$$\begin{aligned} \frac{z}{c} &= C\left(\frac{x}{c}\right) S\left(\frac{x}{c}\right) + \frac{x}{c}\frac{\Delta z_{TE}}{c} \\ C\left(\frac{x}{c}\right) &= \left(\frac{x}{c}\right)^{N_1}\left(1-\frac{x}{c}\right)^{N_2} \quad \text{for} \quad 0 \leq \frac{x}{c} \leq 1 \\ S\left(\frac{x}{c}\right) &= \sum_{i=0}^{n}\left[X_i K_{i,n}\left(\frac{x}{c}\right)^i\left(1-\frac{x}{c}\right)^{n-i}\right] \end{aligned} \tag{7}$$

In this equation, $K_{i,n} = \frac{n!}{i!(n-i)!}$. The exponents N_1 and N_2 are chosen to reflect the desired geometry type. For an airfoil, typically $N_1 = 1/2$ and $N_2 = 1$ are used, as $\sqrt{x/c}$ produces rounded leading edges and $(1-x/c)$ leads to sharp trailing edges. The weight factors X_i represent the design variables. CST parameterization ensures C^2 continuity of the surfaces and effectively captures a range of smooth airfoil shapes. Ten design parameters (five for the upper surface and five for the lower surface) define this parameterization. However, in order to ensure C^2 continuity, the first CST parameter on the lower surface is chosen equivalent to the first parameter on the upper surface, effectively resulting in nine design parameters.

The theoretical range for CST parameters is $[-1, 1]$. We consider design spaces in exploration and exploitation modes bounded relative to the baseline transonic airfoil (RAE2822) design $\boldsymbol{x}_0$. In search of an optimal design away from the baseline, in the exploration mode, we consider the CST bounds at $\boldsymbol{x}_0 \pm 0.3$. Although, these bounds may encounter unrealistic designs, they are also expected to capture a significantly improved (optimal) design. To prevent unrealistic designs and enhance optimizer convergence, in the exploitation mode we consider setting CST bounds at $\boldsymbol{x}_0(1 \pm 0.3)$, i.e., $\pm 30\%$ of the baseline design. Fig. 2 illustrates both the design variable bounds and example airfoil profiles away-from as well as around the baseline.

3.4. Numerical model

The flow around the airfoil is simulated using the TAU CFD solver from the German Aerospace Center (DLR) [26]. The aerodynamic properties of interest are determined by solving the RANS equations along with the $k-\omega$ SST turbulence model [27]. The solver's configuration includes a 4w multigrid cycle, a backward Euler solver for pseudo-time integration and a central flux discretization scheme. An infinite swept-wing formulation for 2.5D analysis is used to efficiently consider cross-flow effects, as detailed in [28]. The employed unstructured mesh comprises 150,000 cells and 1024 surface nodes, as shown in Fig. 3. The wall normal discretization has a growth ratio of 1.05 allowing to maintain a maximum y^+ of 0.25. Laminarity (transition prediction) is considered for upper as well as lower surface of the airfoil. The comparison of results for baseline airfoil simulation and experiments is deferred to the extensive studies in the aerospace community (and thereby its literature) [29].

To predict the transition location on the airfoil, two different methods are utilized: the widely used e^N method [30] and the more recently developed DLR $\gamma-$ model [13]. The aim of employing both models is to compare the resulting optimal designs and evaluate their robustness against environmental and operational uncertainties.

The combination of linear stability theory (LST) and e^N method is considered as state-of-the-art for aerodynamic shape optimization involving laminar flow. This method is validated through wind-tunnel and flight tests [8,24] and frequently employed in the industry for predicting transition. It is, therefore, considered as reference method in the present work and, for brevity, referred to as e^N method. This streamline-based approach is implemented in the transition prediction module of the DLR TAU code [12]. For the present work the option to compute

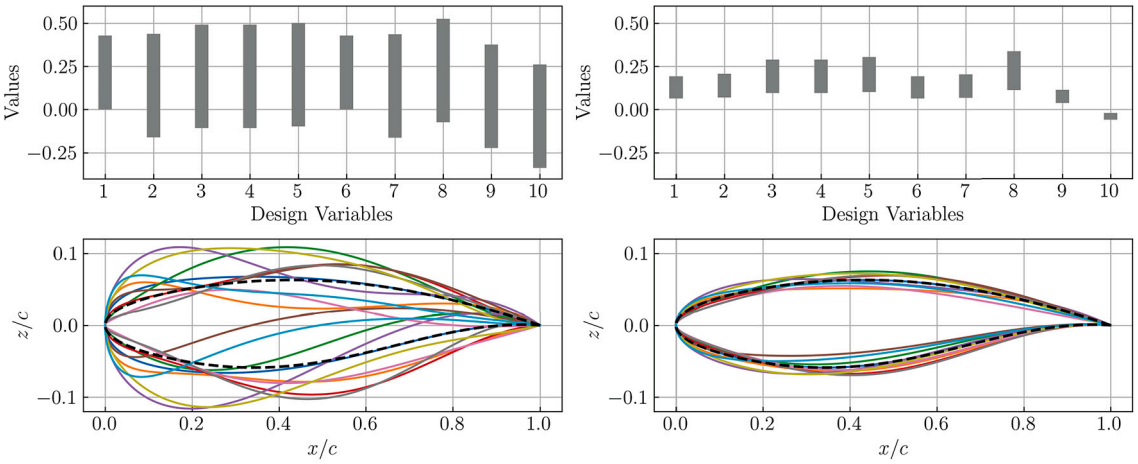

Fig. 2. CST design variable bounds used for optimization in exploration (left) and exploitation (right) modes. RAE2822 airfoil (dashed) and sample airfoil profiles (colored) in the design space (bottom).

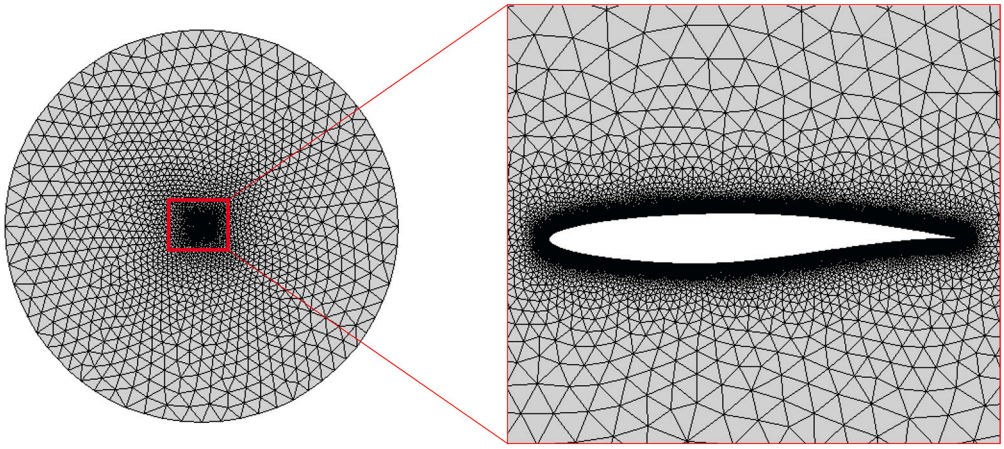

Fig. 3. CFD grid of the baseline (RAE2822) airfoil used in the optimization problem. Every iteration in the optimization performs a mesh deformation.

boundary-layer data with the boundary-layer code COCO [31] is used. Linear stability analysis is performed with the LILO code [32] in incompressible mode. According to the e^N method, the transition location is determined where the N-factors for Tollmien-Schlichting (TS) transition or crossflow (CF) transition exceed certain thresholds.

The class of transition transport models has recently gained significant attention, in particular for application in laminar airfoil design. The DLR γ model [13], an enhancement of the γ-Re_{Θ_t} model, for transport aircraft applications is a member of this class and used as a second transition prediction method in this work. It includes the "Simple-AHD" criterion [33], i.e. an adapted criterion accounting for pressure gradients and considering the effect of compressibility. Furthermore, it includes a crossflow extension [34]. It has been effective for laminar wings at high Reynolds numbers (around 10^7) and is continuously validated and extended [35]. In this study, however, the crossflow extension is not used as the implemented transition criteria are currently not including a dependence on environmental conditions. This restriction is accepted as previous research [16] has shown that crossflow instabilities do not significantly impact transition location under the considered conditions.

The shape modification during optimization is handled through mesh deformation relying on the Flowsimulator framework. Further details on the steps involved and the framework in general can be found in [36].

3.5. Uncertainty characterization

To achieve laminar configurations resilient to variations in environmental and operational conditions, it's crucial to identify and incorporate these factors into the optimization process. The critical N-factors N_{TS}, N_{CF} used in the e^N method serve as a comprehensive indicator of flow quality, as discussed in [37,8]. These factors are significantly influenced by freestream conditions such as cloud presence and disturbance level (turbulent intensity) [38]. Additionally, surface imperfections and acoustic disturbances can have a detrimental impact on laminar flow, i.e. reduce the critical N-factors. Thus, the physical (environmental) uncertainties associated with the e^N method can be represented by variability in these critical N-factors. A recent study [16] explored various distributions of uncertainties in critical N-factors for the robust optimization of a Natural Laminar Flow (NLF) wing. In this study, uncertainties in the N-factors are characterized as two uniformly distributed random variables: $N_{TS} \sim \mathcal{U}[5, 14]$, $N_{CF} \sim \mathcal{U}[4, 11]$.

Similarly, the environmental uncertainties pertaining to the DLR γ model are expressed through variations in the freestream turbulent intensity Tu. A direct relationship between N_{TS} and Tu [39] is utilized to approximate the distribution of turbulent intensity:

$$N_{TS} = -8.43 - 2.4\,ln(Tu) \tag{8}$$

A sampling-based distribution for Tu is constructed using 1000 samples of N_{TS} from the specified uniform distribution. The surface roughness is an important environmental uncertainty having an impact on crossflow

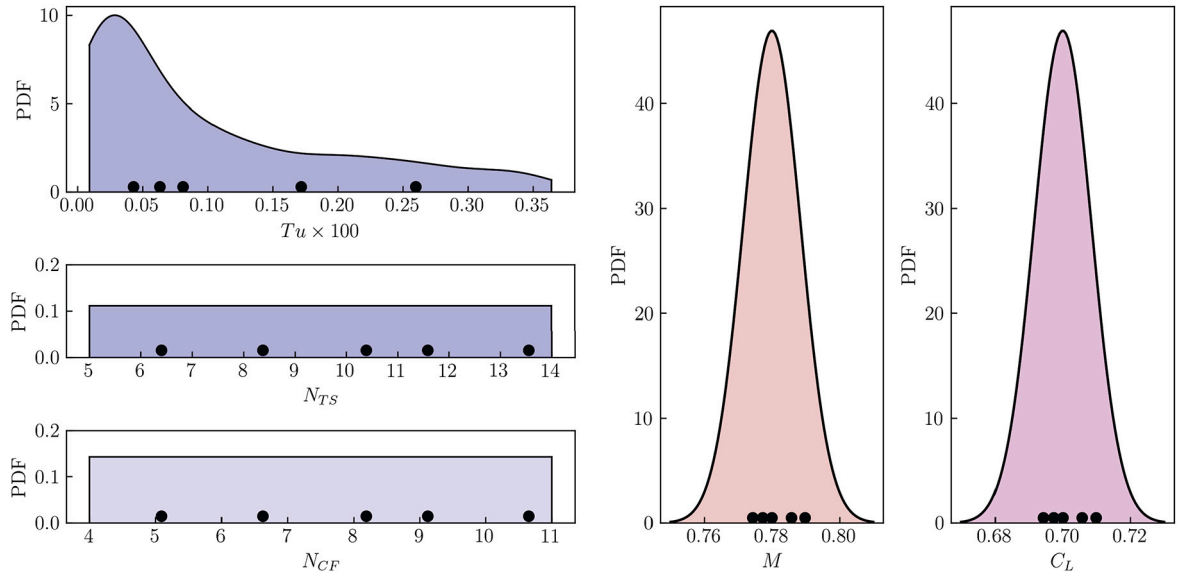

Fig. 4. Distribution of environmental (N_{CF}, N_{TS} and Tu) and operational (M and C_L) uncertainties. For the e^N method the N-factors (N_{TS}, N_{CF}) are considered to be uncertain and turbulent intensity Tu is considered uncertain for the DLR γ model. The dots represent a sampling example based on the distribution.

transition in particular. This effect is reflected by the critical N factor N_{CF} in the e^N method. In case of the optimization with the DLR γ model this effect is neglected, as its implementation was not available at the time of this study. The distributions for the N-factors and freestream turbulent intensity are depicted in Fig. 4 (left).

Typically, Mach number and lift coefficient are considered fixed operational values. However, for short-haul configurations, variability in these conditions during cruise can significantly impact aircraft performance [40]. In this study, the Mach number and lift coefficient are treated as uncertain, modeled using thin symmetric beta distributions centered at the design condition, as illustrated in Fig. 4 (right).

4. Results

In the upcoming subsections, we will present the outcomes of both deterministic and robust optimization in exploration as well as exploitation mode, employing the transition models that were elaborated on in the preceding section.

4.1. Deterministic optimization

The surrogate-based optimization, as detailed in section 2.2.1, is employed to address the deterministic optimization problem formulated in (5). In this scenario, the operational conditions, specifically the Mach number and lift coefficient, are maintained at their design point values of 0.78 and 0.7, respectively. The optimization process also assumes fixed values for the N-factors (used in the e^N method) and turbulent intensity (for the DLR γ model), set at $N_{TS} = 11.5, N_{CF} = 8.5$ and $Tu = 0.0247\%$. The turbulent intensity value is derived from N_{TS} based on the relationship presented in (8). The optimization budget (resource allocation), which includes the number of DoE samples and the infill iterations, is limited to 100 and 20, respectively. This allocation translates to ten samples per DoE with two infill points for each dimension in the ten-dimensional design space $\mathbb{R}^{10}$, a strategy considered effective for creating an accurate meta-model, as noted in [17,16].

In Fig. 5, the optimal design and its pressure profile are compared with those of the baseline configuration (RAE2822) for both the transition models and design spaces. For both transition models employed, the optimal airfoil demonstrates superior performance compared to the baseline, achieving a delayed transition almost up to the shock location. For the design space in exploration mode, as shown in Fig. 5 (a, c), the transition in the optimized airfoil using the e^N method and DLR γ model occurs around 58% and 60%, respectively. This results in a significantly larger area of laminar flow than the baseline configuration, leading to a large reduction in drag – 50% for the e^N method and 52% for the DLR γ model. In exploitation mode, as shown in Fig. 5 (b, d), the transition in the optimized airfoil using the e^N method and DLR γ model occurs around 45% and 42%, respectively. This results in a larger area of laminar flow than the baseline configuration, leading to a notable reduction in drag – 22% for the e^N method and 19% for the DLR γ model. The optimization results in a stronger shock wave as compared to the baseline configuration. This can be attributed to the trade-off between achieving extended laminar flow and managing stronger shock waves. Unlike traditional approaches in the literature that primarily focus on reducing pressure drag, our findings indicate the necessity of balancing both viscous and pressure drag components. A breakdown of drag into its pressure and friction components is presented in Table 1. Compared to the baseline, the pressure drag for optimized airfoils is mainly dominated by the increased wave drag due to stronger shock strengths. However, this increase is effectively offset by reductions in form and viscous drag, resulting in a total drag that remains significantly lower than the baseline. This trade-off underscores the complexity of optimizing transonic airfoil designs, where achieving optimal aerodynamic performance requires carefully balancing these competing factors.

Table 1
Comparison of drag (C_D) with its pressure and viscous components (C_{D_p} and C_{D_f}) for deterministic optimization. The pressure component is further decomposed in wave $C_{D_p,wave}$ and form $C_{D_p,form}$ parts.

Case	C_D, [DC]	$C_{D_p,wave}$, [DC]	$C_{D_p,form}$, [DC]	C_{D_f}, [DC]
e^N method				
Baseline (RAE2822)	97.0	16.2	31.3	49.5
Exploration mode	48.7	20.1	10.1	18.5
Exploitation mode	75.8	31.6	26.8	17.4
DLR γ model				
Baseline (RAE2822)	97.2	14.6	30.1	52.5
Exploration mode	46.6	18.7	8.8	19.1
Exploitation mode	78.7	34.8	24.2	19.7

Despite the complexity of a high-dimensional design space, it's remarkable how the surrogate-based optimization successfully identifies a realistic laminar profile, effectively predicting the transition and minimizing drag within a straightforward constraint framework. The resulting laminar airfoil exhibits a continuous favorable pressure gradient up

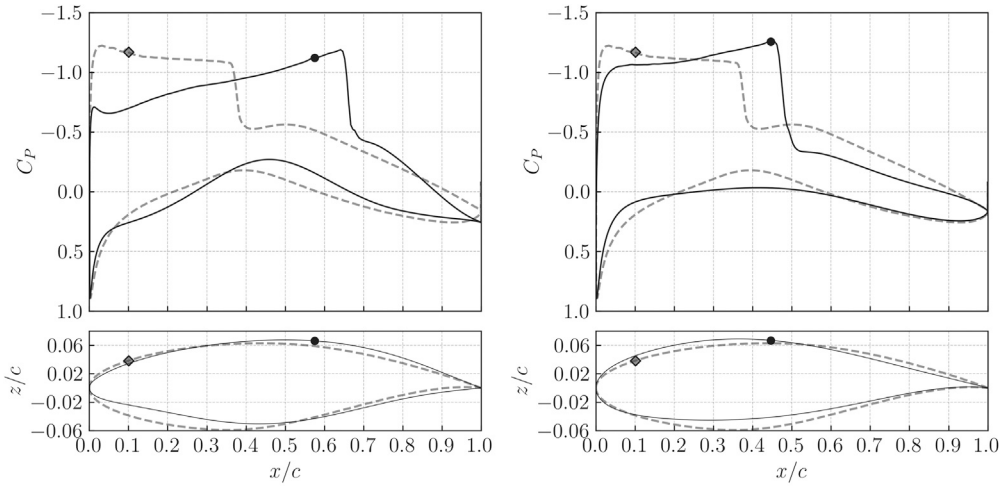

(a) e^N method in exploration mode (b) e^N method in exploitation mode

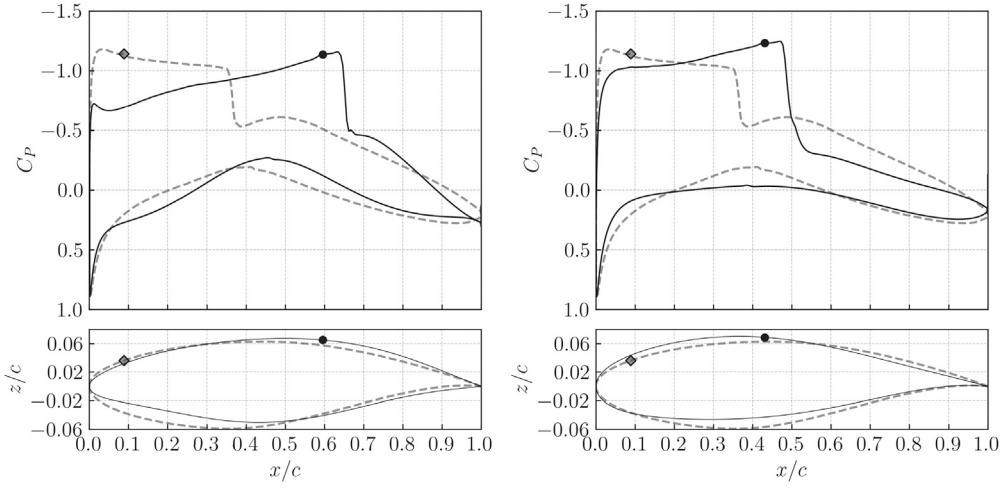

(c) DLR γ model in exploration mode (d) DLR γ model in exploitation mode

Fig. 5. Surface pressure distribution at deterministic optimums for e^N method and DLR γ model using design space in exploration and exploitation modes. The dashed and the solid line represent the baseline (RAE2822) and the optimized airfoil, respectively. The corresponding transition locations (x_{Tr}/c) are denoted by symbols.

to the shock, as expected from previous studies [8]. The differences between the baseline and the optimized profiles for both the e^N method and DLR γ model are small. This is anticipated, given that the DLR γ model is based on the "Simple-AHD" criterion [33], which in turn is based on a database generated using compressible LST. In contrast to that, incompressible LST is used in the present optimization process with the e^N method, which might be the reason for the slight variances compared to the results with the DLR γ model. It is worth noting that the optimization using exploration mode design space, although encountered a large number of unrealistic designs, resulted in a design with larger laminar region as compared to that obtained using exploitation mode design space.

In environments with fluctuating conditions, the performance of an optimal design determined under deterministic assumptions may significantly degrade. The presence of uncertainties can cause the transition location in a deterministic optimum configuration to shift considerably upstream, leading to entirely turbulent flow. To analyze the impact of environmental and operational uncertainties on the aerodynamic efficiency of the deterministic optimum, we adopt a surrogate-based uncertainty quantification method, as outlined in section 2.2.2. A Kriging surrogate model is constructed using five DoE samples plus one infill sample for each random variable. This infill criterion is designed to enhance the surrogate model by focusing on local error estimates (as detailed in section 2.2.2). The mean drag coefficient is calculated using 10,000 Quasi Monte-Carlo samples in the stochastic space evaluated with the surrogate. This is then compared to a reference solution obtained from 200 Monte-Carlo samples directly evaluated using the black-box (CFD solver). The relative error in the mean and standard deviation of the drag coefficient for both transition models and design spaces is less than 1.2% and 2.5%, respectively.

Fig. 6 depicts random realizations of the pressure profiles and transition locations using the deterministic optimum based on exploration and exploitation mode design spaces, incorporating environmental uncertainty - N-factors (for the e^N method) and Tu (for the DLR γ model), and operational uncertainties in Mach number and lift coefficient detailed in section 3.5. For both transition prediction methods in exploration mode (Fig. 6 (a, c)), it is evident that the transition location from laminar to turbulent flow varies significantly, ranging between 5 and 60% for – from near the leading edge to the shock. Consequently, the deterministic optimum operates predominantly in turbulent mode across a wide range of environmental parameters and operational conditions, indicating low resilience to uncertainties. Similarly, the deterministic optimum based on the exploitation mode (Fig. 6 (b, d)) shows that the transition location is highly impacted varying from close to the leading edge up to the

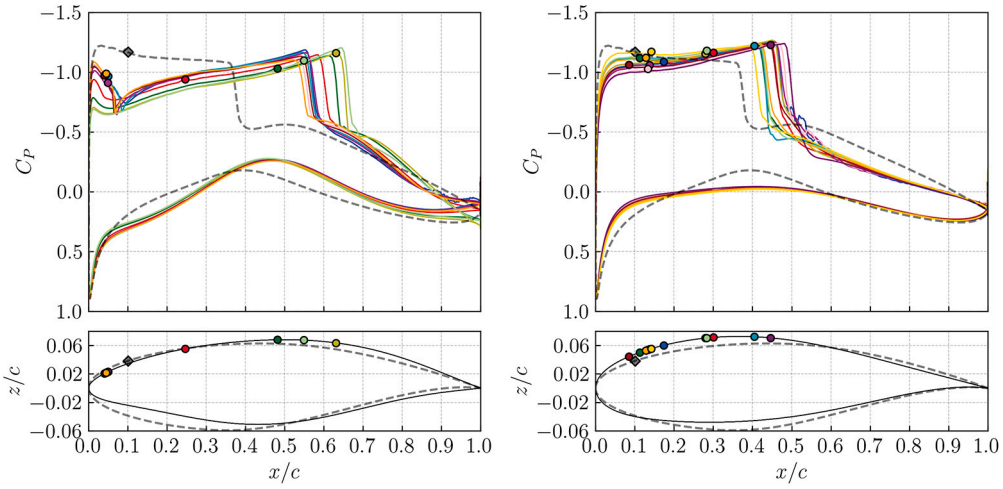

(a) e^N method in exploration mode

(b) e^N method in exploitation mode

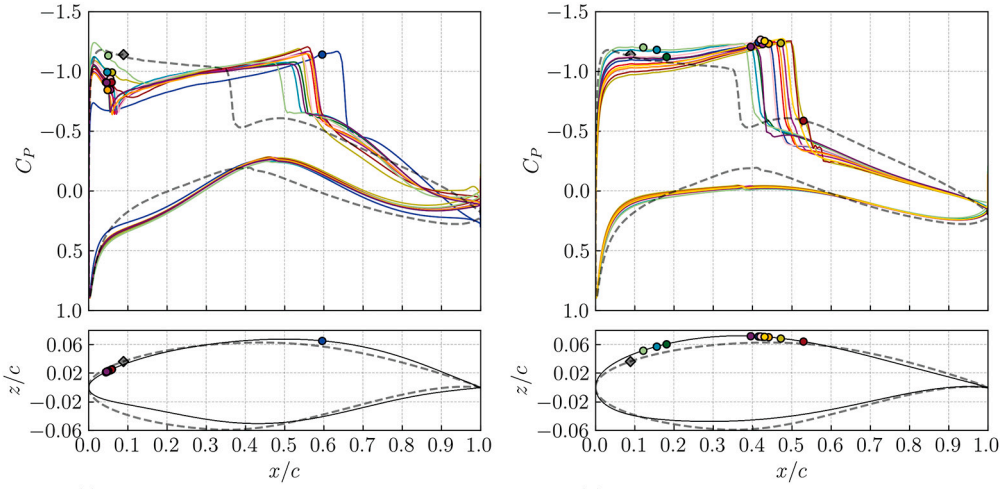

(c) DLR γ model in exploration mode

(d) DLR γ model in exploitation mode

Fig. 6. Random realizations of surface pressure distribution at deterministic optimums for e^N method and DLR γ model under uncertainties using design space in exploration and exploitation modes. The dashed and the solid line represent the baseline (RAE2822) and the optimal airfoil, respectively. The corresponding transition locations (x_{Tr}/c) are denoted by symbols.

shock location, ranging between 10 and 50%. Additionally, the shock wave is observed to be stronger compared to the baseline, adding to the performance issues, particularly when early transition induces fully turbulent flow. Once again, the deterministic optimum operates predominantly in turbulent mode and is highly sensitive to uncertainties. Moreover, the optimum designs based on exploration mode have higher variance in the transition location as compared to the one obtained using exploitation mode. Therefore, although the exploration mode based deterministic optimum offers relatively lower drag (larger laminar region), the performance check reveals its rather unstable behavior under uncertainties. Note that, the pressure distributions used for visualization purposes are based on a few, randomly selected realizations and do not cover the whole range of all evaluated conditions.

4.2. Robust optimization

As previously mentioned, the deterministic optimization approach leads to an unstable configuration where a small variation in environmental uncertainties can significantly impact performance. Hence, we turn to robust optimization, which considers uncertainties (refer to section 2.1). Our method involves using bilevel surrogate-based optimization to minimize the average drag coefficient, taking into account environmental and operational uncertainties. We employed surrogate-based uncertainty quantification in the inner loop to estimate the mean drag coefficient, using five DoE samples and one infill sample per input random variable. In a manner similar to deterministic optimization, we utilized 100 DoE samples with 20 infill iterations for optimization.

Fig. 7 depicts random realizations of the pressure profiles and transition locations using the robust optimum based on exploration and exploitation mode design spaces, incorporating environmental uncertainty - N-factors (for the e^N method) and Tu (for the DLR γ model), and operational uncertainties in Mach number and lift coefficient detailed in section 3.5. For both transition prediction methods in exploration mode (Fig. 7 (a, c)), transition location mostly lie in the range of 45 to 62% for the e^N method and 47 to 59% for the DLR γ model. Similarly, the robust optimum based on the exploitation mode (Fig. 7 (b, d)) shows that transition location mostly lie in the range of 30 to 58% for the e^N method and 42 to 56% for the DLR γ model.

Compared to the baseline and deterministic optimal, the robust optimal design demonstrated a smoother transition location variation and a weaker shock wave. This robust optimal design overall favors a delayed transition, leading to an extended laminar region even under challenging environmental and operational conditions, thereby exhibiting

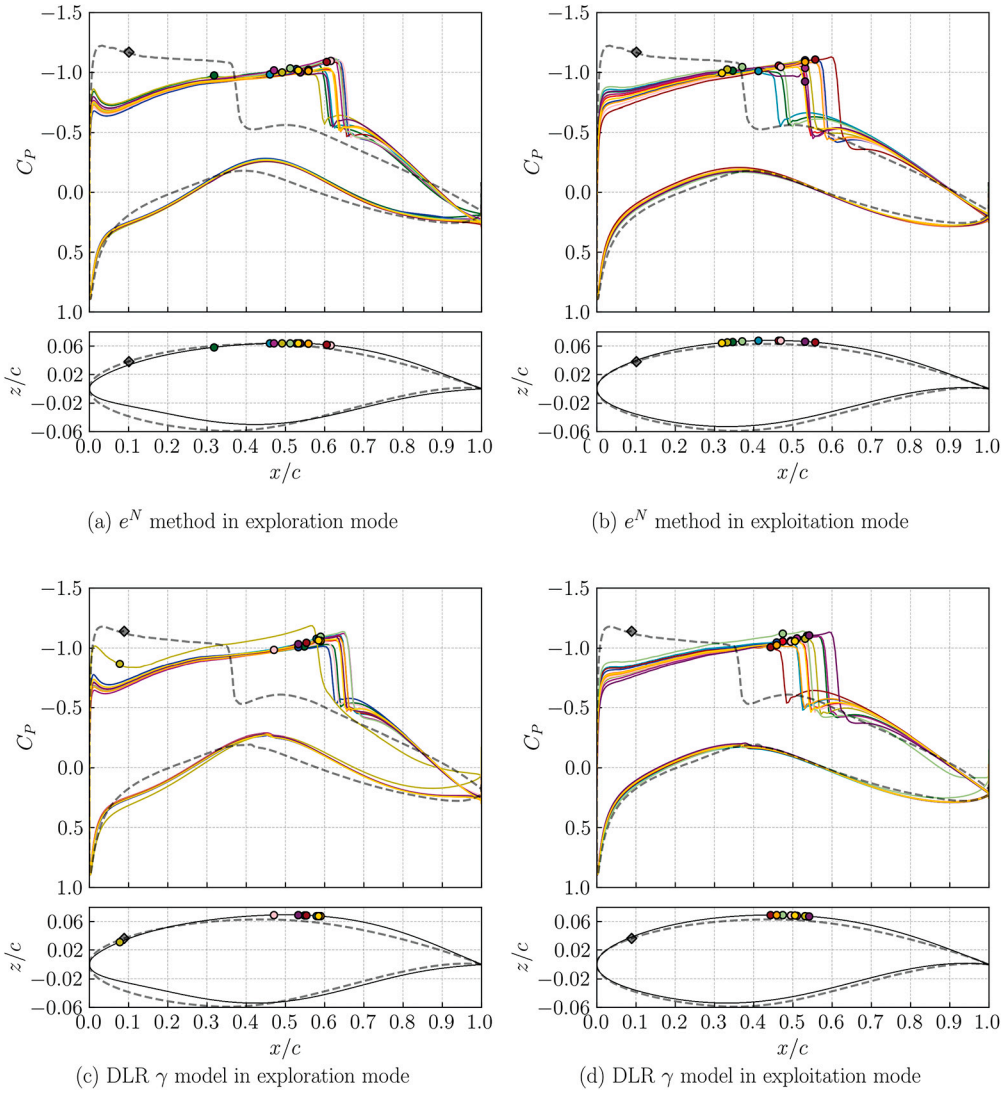

(a) e^N method in exploration mode

(b) e^N method in exploitation mode

(c) DLR γ model in exploration mode

(d) DLR γ model in exploitation mode

Fig. 7. Random realizations of surface pressure distribution at robust optimums for e^N method and DLR γ model under uncertainties using design space in exploration and exploitation modes. The dashed and the solid line represent the baseline (RAE2822) and the optimal airfoil, respectively. The corresponding transition locations (x_{Tr}/c) are denoted by symbols.

greater resilience and considerable robustness against several uncertainties.

Note that a few realizations for robust optimum in exploration mode exhibit transition location close to the leading edge leading into fully turbulent flow. This can again be attributed to the previously discussed unstable behavior of optimal design obtained using exploration mode. This is however acceptable since the standard deviation in transition location over all the realizations is reasonably low. In order to avoid large number of realization with transition locations near the leading edge, one may use a different expectation measure (e.g. $\mu + 3\sigma$) to be minimized.

4.3. Overall performance

Fig. 8 shows polar plots for four key aerodynamic QoIs - angle of attack α, moment coefficient C_M, drag coefficient C_D, and transition location relative to chord length x_{Tr}/c, at deterministic optimums for e^N method and DLR γ model using design space in exploration and exploitation modes. The colored polygons in the graphs represent the normalized values of these QoIs. The extent of variation in the polygon's vertices inversely reflects robustness of the design. It is evident that the deterministic optimum exhibit very high variability in all the QoIs, implying a lack of robustness against uncertainties. In particular, for both the transition models, the design obtained using exploration mode is highly unstable as compared to the ones obtained with exploitation modes. Fig. 9 shows the polar plots at robust optimums for e^N method and DLR γ model using design space in exploration and exploitation modes. Contrary to the deterministic optimums, the robust optimum demonstrate significantly lower variability across QoIs. Overall, the design obtained using exploration mode is only slightly more unstable as compared to the ones obtained with exploitation modes. The polar plot for DLR γ model in the exploration mode does not seem to be robust at first due to a realization with significantly larger drag coefficient (more upstream transition location). However, if we consider the polar plot without this realization, then the overall robustness of this design is significantly higher than its deterministic counterpart.

Fig. 10 depicts the violin plots for drag coefficient obtained from several realizations at deterministic and robust optimums under uncertainties for both the e^N method and the DLR γ model using exploration and exploitation modes of design space. For all the deterministic optimums, the violin plots show that the mean drag coefficient is close to the baseline (RAE2822) drag. The distributions span over a large range of drag values implying a larger variability due to the wide scattering of transition locations, as shown in Fig. 6. For instance, the bimodal

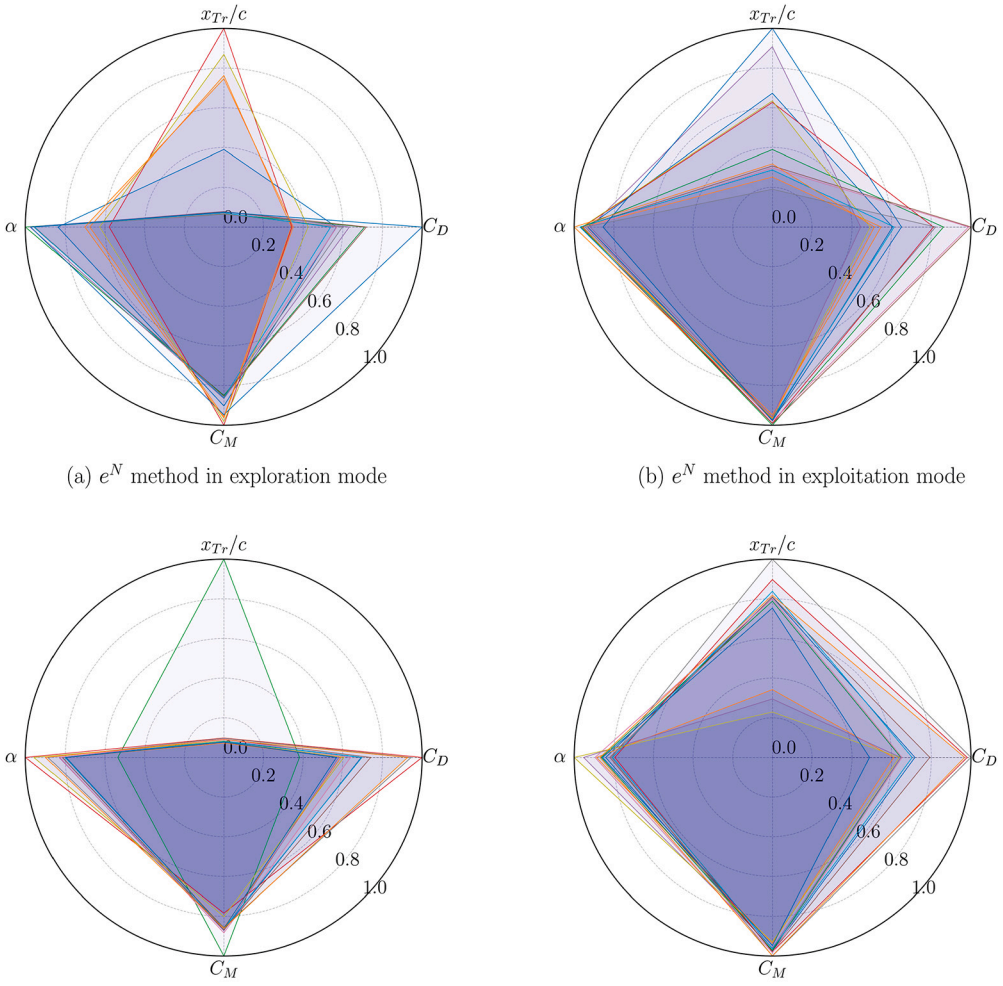

(a) e^N method in exploration mode

(b) e^N method in exploitation mode

(c) DLR γ model in exploration mode

(d) DLR γ model in exploitation mode

Fig. 8. Polar graphs of four aerodynamic QoIs - angle of attack α, moment coefficient C_M, drag coefficient C_D and transition location w.r.t. chord length x_{Tr}/c, at deterministic optimums for e^N method and DLR γ model using design space in exploration and exploitation modes. The polygons (colored) represent the realizations of the normalized QoIs.

distribution for e^N method in the exploration mode has a high probability mode towards the higher levels of drag count (indicating large portion of realizations with significant loss of laminar flow) while the low probability mode lies towards the lower levels of drag count (indicating only a few realizations with extensive laminarity). The violin plots for robust optimums demonstrate a significant reduction in mean drag counts as compared to the baseline and the deterministic counterparts. The distributions span over a relatively small range of drag values with a near-deterministic (low variance) drag count observed for the optimums in the exploration. This can be attributed to the more concise scattering of transition locations, as shown in Fig. 7. The distribution for DLR γ model in the exploration mode shows a long tail towards the higher values of drag due to the presence of a few realizations that lead to early transition (as discussed earlier).

Fig. 11 shows the Sobol indices for drag coefficient (C_D) and transition location (x_{Tr}/c) based on uncertainty quantification using robust optimums obtained with design space in exploration and exploitation modes for both e^N method and DLR γ model. Sobol indices are a method in global sensitivity analysis that uses variance to decompose the model output variance into fractions attributable to different inputs or combinations of inputs. Further details on estimating Sobol indices are deferred to Appendix B. Under the considered uncertainties (see section 3.5), the sensitivities indicate that drag coefficient and transition location are predominantly influenced by the variability in Mach number, and Tollmien-Schlichting N-factor and turbulence intensity for e^N method and DLR γ model, respectively. In particular, for the optimized result based on the DLR γ model, the influence of turbulence intensity on the drag coefficient is dominant over Mach number. The influence of the variability in the crossflow N-factor is rather small which is also in accordance with a previous research [16] that has shown that crossflow instabilities do not significantly impact transition location under similar conditions.

In this study, the overall precision of the optimization is influenced by several factors, with the accuracy of predicting transition being paramount. The intermittency-based model recently developed for predicting transition location showed high accuracy, closely matching the results from the reference method (LST/e^N method). Consequently, the optimal airfoil shapes derived using the DLR γ model closely resembled those obtained using the e^N method, whether deterministic or robust. The total number of black-box evaluations directly affects the optimization process cost. Conducting a single evaluation requires about 45 minutes for the e^N method and 25 minutes for the DLR γ model, using 128 processors. While this computational cost is relatively minor during the DoE phase due to its parallelizability, the expense escalates with the increase in sequential infill samples. Therefore, the DLR γ model, with its integrated on-the-fly transition prediction capability, is more efficient than the e^N method, which depends on periodic convergence in x_{Tr}. Moreover, the intermittency-based transition transport model requires a low number of parameter settings. Consequently, given these

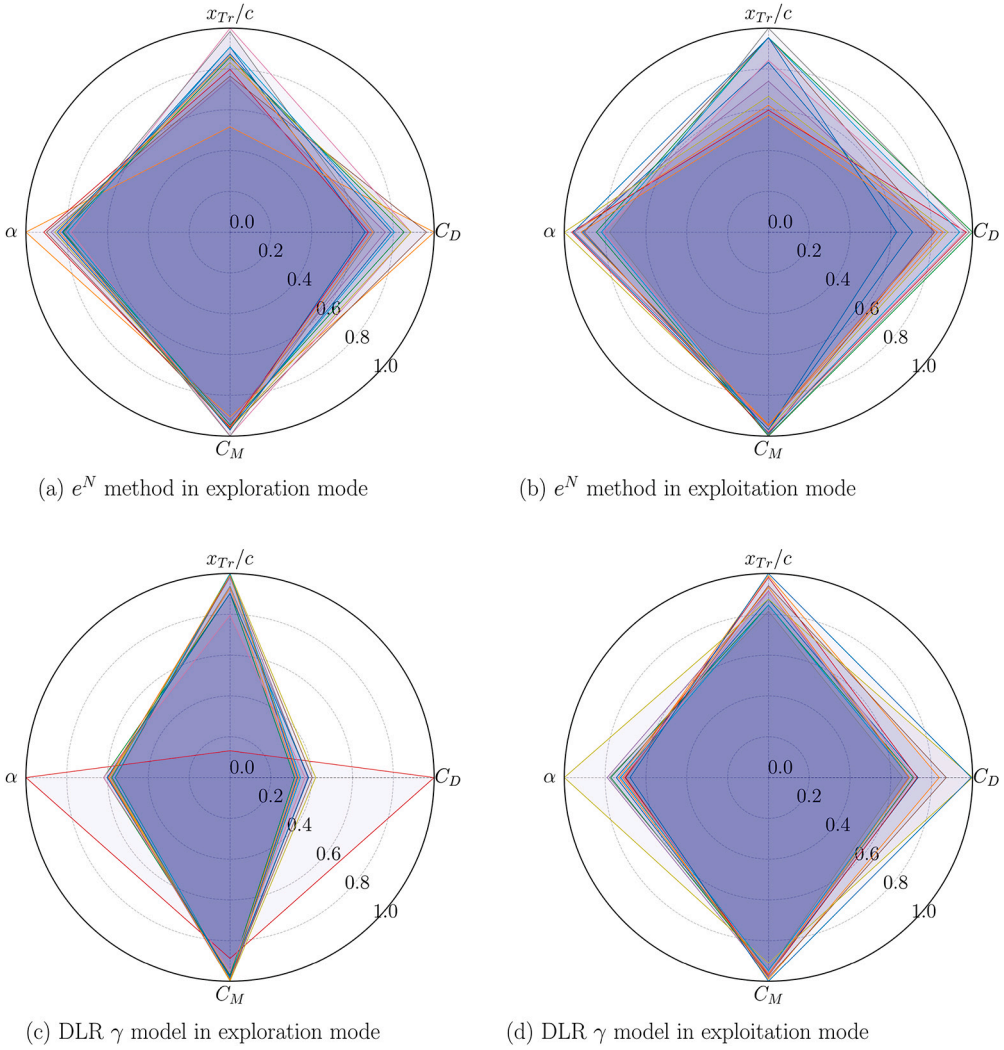

(a) e^N method in exploration mode (b) e^N method in exploitation mode

(c) DLR γ model in exploration mode (d) DLR γ model in exploitation mode

Fig. 9. Polar graphs of four aerodynamic QoIs - angle of attack α, moment coefficient C_M, drag coefficient C_D and transition location w.r.t. chord length x_{Tr}/c, at robust optimums for e^N method and DLR γ model using design space in exploration and exploitation modes. The polygons (colored) represent the realizations of the normalized QoIs.

factors, the DLR γ model emerges as a more suitable option for conducting robust optimization studies, which are inherently costly.

A few remarks can be drawn about optimization (deterministic or robust) using exploration and exploitation design modes. In general, the extent of the laminar region was found to be larger for the designs obtained using exploration mode resulting in lower drag. On the contrary, the optimal designs obtained using exploitation mode were found to be more stable with lower variability in transition location and drag count. Exploitation mode optimization is akin to traditional optimization, focusing on incremental improvements around an initial baseline design. In contrast, optimization using exploration mode represents a more disruptive approach, aiming for high-performance designs that may significantly deviate from the baseline.

5. Conclusions

The potential gains in fuel efficiency from laminar designs might not be fully realized in practical scenarios when using common inverse design methods. For laminar airfoils (wings) to maintain high fuel efficiency, they must be robustly designed to withstand environmental and operational uncertainties. Direct optimization helps create realistic designs that promote laminarity up to or near the shock location, thus delaying transition and reducing drag. However, since these configurations are optimized at nominal values, they become unstable under varying environmental and operational conditions, often leading to significant loss of laminar flow. This issue can be addressed by quantifying uncertainties, projecting them onto QoIs, and using their statistics for optimization, resulting in designs resilient to changes in environmental and operational factors.

In our study, a robust optimization framework was employed to enhance the natural laminar flow region of an infinite swept wing using exploration and exploitation mode design spaces. Initial deterministic optimization revealed that the optimum designs were not robust against environmental uncertainties for both transition prediction methods (e^N method and DLR γ model) and both the design spaces. However, incorporating uncertainties into the optimization process, particularly using a surrogate-based approach, significantly improved average performance and yielded robust designs. These designs featured delayed transitions (extended laminarity), weaker shock waves, realistic pressure profiles, and stability. Moreover, robust optimums encouraged more gradual changes in the transition location when subject to uncertainties, compared to the more significant loss of laminar flow obtained with the deterministic optimums. For efficient robust optimization, the DLR γ transition transport model was more cost-effective and user-friendly than the traditional e^N method. Moreover, it was observed that, although the optimum designs from exploration mode generally have a larger laminar region, the optimum designs from exploitation mode tend to be more stable i.e. higher resilience against uncertainties.

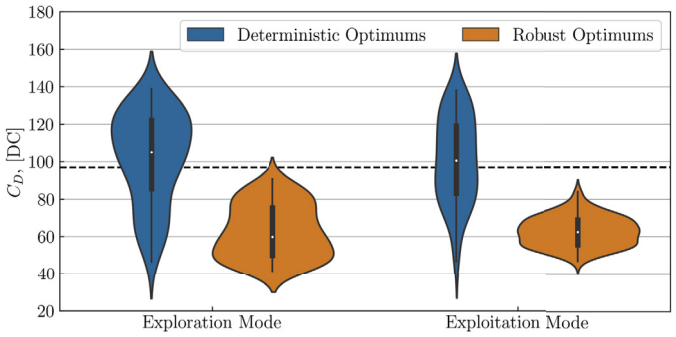

(a) e^N method drag count distributions

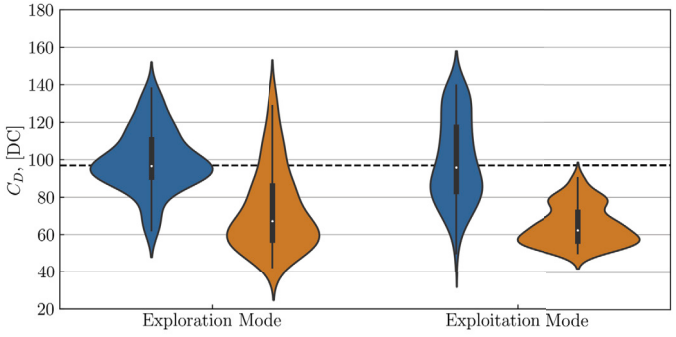

(b) DLR γ model drag count distributions

Fig. 10. Violin plot for drag predictions at deterministic and robust optimums under uncertainties using design space in exploration and exploitation mode for both e^N method and DLR γ model. The dashed line represents the baseline (RAE2822) drag count.

Future research could explore replacing the thickness constraint with a wing-box constraint which might yield more realistic designs. Considering other uncertainties, like variability in Reynolds number or model form uncertainties, could also be beneficial. Additionally, this study can be extended towards laminar wing design focusing on blending optimized wing sections (airfoils).

CRediT authorship contribution statement

Jigar Parekh: Writing – review & editing, Writing – original draft, Visualization, Software, Methodology, Investigation, Formal analysis, Data curation, Conceptualization. **Philipp Bekemeyer:** Writing – review & editing, Supervision, Resources, Project administration, Funding acquisition, Conceptualization. **Sebastian Helm:** Writing – review & editing, Validation, Methodology, Conceptualization. **Daniela Gisele François:** Validation, Methodology, Conceptualization. **Cornelia Grabe:** Writing – review & editing, Resources, Project administration, Funding acquisition.

Declaration of competing interest

The authors declare the following financial interests/personal relationships which may be considered as potential competing interests: Jigar Parekh reports financial support was provided by German Research Foundation. If there are other authors, they declare that they have no known competing financial interests or personal relationships that could have appeared to influence the work reported in this paper.

Data availability

The authors do not have permission to share data.

Acknowledgements

The funding of parts of these investigations from the Deutsche Forschungsgemeinschaft (DFG, German Research Foundation) under Germany's Excellence Strategy—EXC 2163/1-Sustainable and Energy Efficient Aviation—Project-ID 390881007 is gratefully acknowledged. The authors highly acknowledge Thomas Streit and Gokul Subbian from

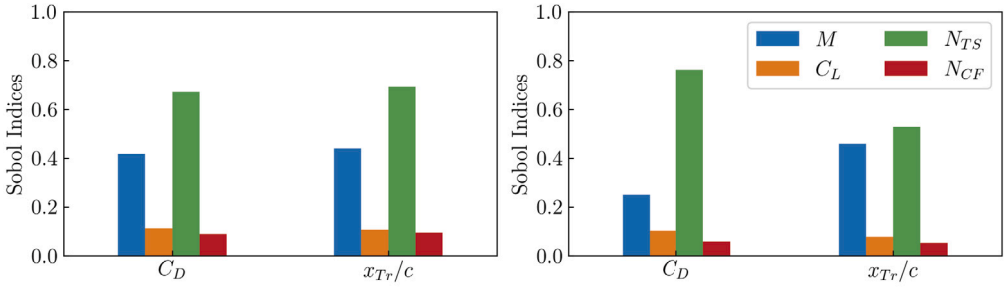

(a) e^N method Sobol indices for robust optimum

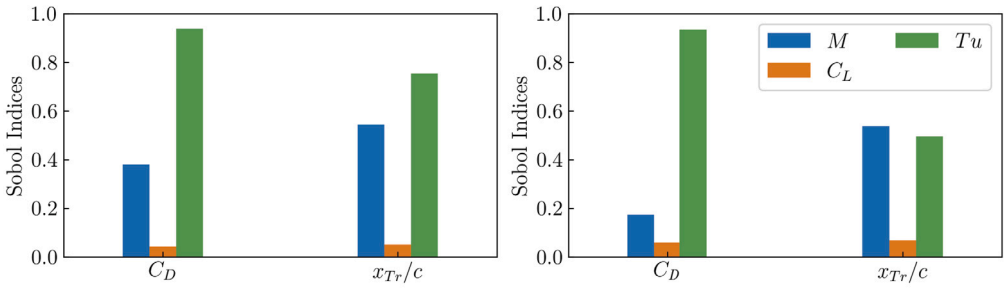

(b) DLR γ model Sobol indices for robust optimum

Fig. 11. Sobol indices for drag coefficient (C_D) and transition location (x_{Tr}/c) based on uncertainty quantification using robust optimums obtained with design space in exploration (left) and exploitation (right) modes for both e^N method and DLR γ model.

German Aerospace Center (DLR) for their support in the drag decomposition steps and for their insightful discussions.

Appendix A. Gaussian process regression

We summarize the steps involved in the construction of a Kriging surrogate model using SMARTy. For more details, the reader is referred to the literature [41] and the references therein. A basic assumption of the Kriging approach is that the true functional relationship $y : \mathcal{D} \to \mathbb{R}$ between the input variables $x \in \mathcal{D} \subseteq \mathbb{R}^d$ and their corresponding scalar-valued output $y(x) \in \mathbb{R}$ is a realization of a random function,

$$\mathcal{Y}(x) = g(x)\beta + \epsilon(x), \tag{A.1}$$

where $g : \mathbb{R}^d \to \mathbb{R}^p$ is a known regression model, β is a vector of unknown regression parameters, and $\epsilon(x)$ is a Gaussian process with zero mean and known covariance structure. Covariance is given by a known stationary spatial correlation kernel:

$$\mathrm{Cov}[\epsilon(x), \epsilon(x')] = \sigma^2 R_\theta(x, x'), \tag{A.2}$$

with $R_\theta(x, x')$ being the correlation kernel and σ^2 representing the process variance. Different types of covariance functions are implemented in SMARTy. In this work we use a *Gaussian Exponential* kernel [42]:

$$R_\theta(x, x') = \prod_{k=1}^{m} \exp(-\theta_k |x_k - x'_k|^{p_k}), \quad \text{with } \theta_k \in \mathbb{R}_+,\ p_k \in [1, 2],\ k = 1, ..., m \tag{A.3}$$

where θ are the unknown correlation parameters [43].

The Kriging predictor is determined as the best linear unbiased estimator and can be rewritten as,

$$\hat{y}(x) = g(x)\hat{\beta} + r(x)^\top R^{-1}(Y - F\hat{\beta}), \tag{A.4}$$

where R is the correlation matrix, Y is the vector of observed data, F is the matrix of regression vectors, $r(x)$ is the vector of correlations between sample locations and the new location x, and $\hat{\beta} = (F^T R^{-1} F)^{-1} F^T R^{-1} Y$.

The choice of the correlation parameters θ has a large impact on the Kriging predictor. Therefore, it is usually determined by a maximum likelihood prediction [44]. Using the likelihood-optimal parameters the mean squared error (MSE) of Kriging estimator at a location $x \in \mathcal{D}$ is given by [45],

$$\mathrm{MSE}(x) = \sigma^2(1 + u^\top (F^\top R^{-1} F)^{-1} u - r(x)^\top R^{-1} r(x)), \tag{A.5}$$

with $u = F^\top R^{-1} r(x) - f(x)$, providing an estimate of the prediction error variance at location x.

Appendix B. Global sensitivities in terms of Sobol indices

Sobol indices are a variance-based global sensitivity analysis approach which decomposes the variance of the model output into fractions which can be associated to the inputs or sets of inputs. This method analyzes the influence of each component of an input random vector $X = (X^1, ..., X^{n_X})$ on an output random variable Y by computing Sobol' indices [46].

Consider f as the physical model such as $Y = f(\mathbf{X})$. For any subset $I \subseteq \{1, \dots, n_x\}$, with $\mathbf{X}_I = (X_i)_{i \in I}$, the variance of Y as a function of $\mathbf{X} = (X^1, \dots, X^{n_x})$ can be expressed using the Hoeffding decomposition [47] $\mathrm{Var}[Y] = \sum_{I \subseteq \{1,\dots,n_X\}} V_I$, where $V_I = \mathrm{Var}\left[\sum_{J \subseteq I} (-1)^{|I|-|J|} \mathbb{E}[Y|\mathbf{X}_J]\right]$. For better readability, for any integers $1 \le i, j \le n_x$, we define $\tilde{V}_i = V_{\{i\}}$ and $\tilde{V}_{i,j} = V_{\{i,j\}}$. Thus, we have:

$$\tilde{V}_i = \mathrm{Var}[\mathbb{E}[Y|X_i]], \tag{B.1}$$

$$\tilde{V}_{i,j} = \mathrm{Var}[\mathbb{E}[Y|X_i, X_j]] - \mathbb{E}[Y|X_i] - \mathbb{E}[Y|X_j] \tag{B.2}$$

$$= \mathrm{Var}[\mathbb{E}[Y|X_i, X_j]] - \tilde{V}_i - \tilde{V}_j \tag{B.3}$$

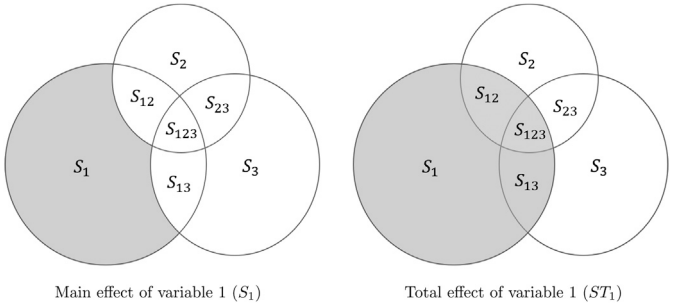

Fig. B.12. Venn diagrams of variance fractions in a three-variable model highlighting Sobol indices of variable 1.

for $i = 1, \dots, n_X$. Thus, the variance of Y can also be written as

$$\mathrm{Var}[Y] = \sum_{i=1}^{n_X} V_i + \sum_{1 \le i < j}^{n_x} V_{i,j} + \dots + V_{12\dots n_X}. \tag{B.4}$$

Since, $\mathrm{Var}[Y] = \sum_{I \subseteq \{1,\dots,n_X\}} V_I$, a result for the sensitivities can be simply derived by dividing both sides by $\mathrm{Var}[Y]$:

$$\sum_{i=1}^{n_X} S_i + \sum_{1 \le i < j \le n_X} S_{i,j} + \dots + S_{1,2,\dots,n_X} = 1 \tag{B.5}$$

The above decomposition of variance shows how the variance of the output can be decomposed into terms associated to each input, as well as to the interactions between them. Sobol indices for first and second order effects are defined as follows; for $i, j = 1, \dots, n_X$, $S_i = V_i / \mathrm{Var}[Y]$ and $S_{i,j} = V_{i,j} / \mathrm{Var}[Y]$. The first order Sobol index S_i represents the contribution towards the variance of Y explained by X_i alone, while the second order Sobol index $S_{i,j}$ represents the contribution towards the variance of Y explained by the interaction of X_i and X_j.

In order to formulate the total order Sobol indices, we define

$$VT_i = \sum_{\substack{I \\ i \in I}} V_I, \quad V_{-i} = \mathrm{Var}[\mathbb{E}[Y|X_1, \dots, X_{i-1}, X_{i+1}, \dots, X_n]] \tag{B.6}$$

for any $i = 1, \dots, n_X$. The $-i$ notation indicates the set of all variables except X_i. Total order Sobol indices are then defined as $ST_i = VT_i / \mathrm{Var}[Y] = 1 - V_{-i} / \mathrm{Var}[Y]$ for $i = 1, \dots, n_X$. The total order Sobol index ST_i is the contribution towards the part of the variance of Y that represents the effect of X_i and its interactions with all the other input variables.

Fig. B.12 shows the Venn diagrams of variance fractions in a three-variable model highlighting the Sobol indices of variable 1. We use numerical methods that rely on independent (Quasi) Monte Carlo realizations of the random vector using a surrogate model to estimate the sensitivities formulated above [48].

References

[1] Publications Office of the European Union, Flightpath 2050: Europe's vision for aviation: maintaining global leadership and serving society's needs, https://op.europa.eu/en/publication-detail/-/publication/296a9bd7-fef9-4ae8-82c4-a21ff48be673, 2011, https://doi.org/10.2777/50266.

[2] North Atlantic Treaty Organization. Advisory Group for Aerospace Research and Development. Fluid Dynamics Panel, Von Karman Institute for Fluid Dynamics, Aircraft Drag Prediction and Reduction, AGARD report, North Atlantic Treaty Organization, Advisory Group for Aerospace Research and Development, 1985, https://books.google.de/books?id=-OTTzgEACAAJ.

[3] G. Redeker, K.H. Horstmann, H. Köster, P. Thiede, J. Szodruch, Design of a natural flow glove for a transport aircraft, in: AIAA CP 907, AIAA, 1990, pp. 375–384, https://elib.dlr.de/35810/, lIDO-Berichtsjahr=1990, pages=10.

[4] D. McLean, Understanding Aerodynamics, 2013, pp. 380–382.

[5] G. Schrauf, Evaluation of the A320 hybrid laminar fin experiment, https://api.semanticscholar.org/CorpusID:112729979, 2000.

[6] R.L. Campbell, M.N. Lynde, Natural laminar flow design for wings with moderate sweep, https://arc.aiaa.org/doi/abs/10.2514/6.2016-4326, 2016, https://doi.org/10.2514/6.2016-4326.

[7] M.N. Lynde, R.L. Campbell, M.B. Rivers, S.A. Viken, D.T. Chan, A.N. Watkins, S.L. Goodliff, Preliminary results from an experimental assessment of a natural laminar flow design method, in: AIAA Scitech 2019 Forum, 2019, https://arc.aiaa.org/doi/10.2514/6.2019-2298.

[8] T. Streit, S. Wedler, M. Kruse, DLR natural and hybrid transonic laminar wing design incorporating new methodologies, Aeronaut. J. 119 (2015) 1303–1326, https://doi.org/10.1017/S0001924000011283.

[9] S.N. Skinner, H. Zare-Behtash, State-of-the-art in aerodynamic shape optimisation methods, Appl. Soft Comput. 62 (2018) 933–962, https://doi.org/10.1016/J.ASOC.2017.09.030.

[10] Z.H. Han, J. Chen, K.S. Zhang, Z.M. Xu, Z. Zhu, W.P. Song, Aerodynamic shape optimization of natural-laminar-flow wing using surrogate-based approach, AIAA J. 56 (2018) 2579–2593, https://doi.org/10.2514/1.J056661, https://arc.aiaa.org/doi/10.2514/1.J056661.

[11] Z. Huan, G. Zheng-Hong, W. Chao, G. Yuan, Robust design of high speed natural-laminar-flow airfoil for high lift, in: AIAA SciTech Forum - 55th AIAA Aerospace Sciences Meeting, 2017, https://arc.aiaa.org/doi/10.2514/6.2017-1414.

[12] A. Krumbein, N. Krimmelbein, G. Schrauf, Automatic transition prediction in hybrid flow solver, part 1: methodology and sensitivities, J. Aircr. 46 (2009) 1176–1190, https://doi.org/10.2514/1.39736.

[13] D.G. François, A. Krumbein, N. Krimmelbein, C. Grabe, Simplified stability-based transition transport modeling for unstructured computational fluid dynamics, J. Aircr. (2023) 1–12.

[14] R.D. Joslin, Aircraft laminar flow control 1, Annu. Rev. Fluid Mech. 30 (1998) 1–29, www.annualreviews.org.

[15] J. Hollom, N. Qiny, Robustness of natural laminar flow airfoil drag optimization to transition amplification factor, in: 18th AIAA/ISSMO Multidisciplinary Analysis and Optimization Conference, 2017, p. 2017, https://arc.aiaa.org/doi/10.2514/6.2017-3144.

[16] C. Sabater, P. Bekemeyer, S. Görtz, Robust design of transonic natural laminar flow wings under environmental and operational uncertainties, AIAA J. 60 (2022) 767–782, https://doi.org/10.2514/1.J060676.

[17] C. Sabater, P. Bekemeyer, S. Görtz, Efficient bilevel surrogate approach for optimization under uncertainty of shock control bumps, AIAA J. 58 (2020) 5228–5242, https://doi.org/10.2514/1.J059480.

[18] A.I. Forrester, A.J. Keane, Recent advances in surrogate-based optimization, Prog. Aerosp. Sci. 45 (2009) 50–79, https://doi.org/10.1016/j.paerosci.2008.11.001, https://www.sciencedirect.com/science/article/pii/S0376042108000766.

[19] P. Bekemeyer, A. Bertram, D.A.H. Chaves, M.D. Ribeiro, A. Garbo, A. Kiener, C.S. Campomanes, M. Stradtner, S. Wassing, M. Widhalm, S. Görtz, F. Jäckel, R. Hoppe, N. Hoffmann, Data-Driven Aerodynamic Modeling Using the DLR SMARTy Toolbox, American Institute of Aeronautics and Astronautics Inc, AIAA, 2022.

[20] I. Sobol', On the distribution of points in a cube and the approximate evaluation of integrals, USSR Comput. Math. Math. Phys. 7 (1967) 86–112, https://doi.org/10.1016/0041-5553(67)90144-9, https://www.sciencedirect.com/science/article/pii/0041555367901449.

[21] Z.-H. Han, S. Görtz, R. Zimmermann, Improving variable-fidelity surrogate modeling via gradient-enhanced Kriging and a generalized hybrid bridge function, Aerosp. Sci. Technol. 25 (2013) 177–189, https://doi.org/10.1016/j.ast.2012.01.006, https://www.sciencedirect.com/science/article/pii/S127096381200017X.

[22] D.R. Jones, M. Schonlau, W.J. Welch, Efficient global optimization of expensive black-box functions, J. Glob. Optim. 13 (1998) 455–492, https://doi.org/10.1023/A:1008306431147/METRICS, https://link.springer.com/article/10.1023/A:1008306431147.

[23] G. Schrauf, Status and perspectives of laminar flow, Aeronaut. J. 109 (2005) 639–644, https://doi.org/10.1017/S000192400000097X, https://www.cambridge.org/core/journals/aeronautical-journal/article/status-and-perspectives-of-laminar-flow/BC5EE06B4032AC2D494AC3518BA0BAD3.

[24] G. Schrauf, Large-scale laminar flow tests evaluated with linear stability theory, J. Aircr. 41 (2012) 224–230, https://doi.org/10.2514/1.9280, https://arc.aiaa.org/doi/10.2514/1.9280.

[25] B.M. Kulfan, Universal parametric geometry representation method, J. Aircr. 45 (2012) 142–158, https://doi.org/10.2514/1.29958, https://arc.aiaa.org/doi/10.2514/1.29958.

[26] T. Gerhold, Overview of the hybrid RANS code TAU, in: MEGAFLOW - Numerical Flow Simulation for Aircraft Design, 2005, pp. 81–92, https://link.springer.com/chapter/10.1007/3-540-32382-1_5.

[27] F.R. Menter, M. Kuntz, R. Langtry, Ten years of industrial experience with the sst turbulence model, in: Turbulence, Heat and Mass Transfer, vol. 4, 2003, pp. 625–632.

[28] J. Drofelnik, A.D. Ronch, 2.5D+ TAU User Guide, DLR, German Aerospace Center TR, 2017.

[29] S. Langer, An initial investigation of solving RANS equations in combination with two-equation turbulence models, Technical Report, Institut für Aerodynamik und Strömungstechnik, 2019, https://elib.dlr.de/129170/.

[30] J.V. Ingen, A suggested semi-empirical method for the calculation of the boundary layer transition region, 1956.

[31] G. Schrauf, COCO—a Program to Compute Velocity and Temperature Profiles for Local and Nonlocal Stability Analysis of Compressible, Conical Boundary Layers with Suction, ZARM TR, 1998.

[32] G. Schrauf, LILO 2.1–User's Guide and Tutorial, GSSC TR 6, Bremen, Germany, Sept. 2004, modified for Ver. 2.1, 2006.

[33] J. Perraud, H. Deniau, G. Casalis, Overview of transition prediction tools in the elsa software, in: ECCOMAS 2014, 2014.

[34] D.G. François, A. Krumbein, N. Krimmelbein, Crossflow extension of a simplified transition transport model for three-dimensional aerodynamic configurations, in: AIAA AVIATION Forum, 2022.

[35] S. Helm, D.G. François, C. Grabe, J. Parekh, P. Bekemeyer, CFD-basierte Transitionsvorhersage für den Entwurf von Laminarflugzeugen (abstract accepted), in: DLRK, 2023.

[36] L. Reimer, R. Heinrich, M. Ritter, A. Krumbein, S. Geisbauer, S. Goertz, T. Leicht, Virtual aircraft technology integration platform: ingredients for multidisciplinary simulation and virtual flight testing, https://arc.aiaa.org/doi/abs/10.2514/6.2021-1202, 2021, https://doi.org/10.2514/6.2021-1202.

[37] G. Schrauf, Industrial view on transition prediction, in: Recent Results in Laminar-Turbulent Transition, 2004, pp. 111–122, https://link.springer.com/chapter/10.1007/978-3-540-45060-3_9.

[38] M. Kruse, A. Küpper, R. Petzold, F. Munoz, Determination of the critical cross flow N-factor for the low-speed wind tunnel braunschweig (DNW-NWB), in: Notes on Numerical Fluid Mechanics and Multidisciplinary Design, vol. 136, 2018, pp. 251–261, https://link.springer.com/chapter/10.1007/978-3-319-64519-3_23.

[39] L.M. Mack, Transition prediction and linear stability theory, ltt, https://ui.adsabs.harvard.edu/abs/1977ltt..agarQ....M/abstract, 1977.

[40] R. Radespiel, W. Heinze, SFB 880: fundamentals of high lift for future commercial aircraft, CEAS Aeronaut. J. (2014), https://doi.org/10.1007/s13272-014-0103-6.

[41] C.M. Bishop, Pattern Recognition and Machine Learning, Springer, 2006.

[42] J. Sacks, W.J. Welch, T.J. Mitchell, H.P. Wynn, Design and analysis of computer experiments, Stat. Sci. 4 (1989) 409–423, https://doi.org/10.1214/ss/1177012413.

[43] Alexander I.J. Forrester, András Sóbester, A.J. Keane, Engineering design via surrogate modelling: a practical guide, in: Engineering Design via Surrogate Modelling, 2008.

[44] A. Bertram, Data-driven variable-fidelity reduced order modeling for efficient vehicle shape optimization, https://doi.org/10.24355/dbbs.084-201811231243-0, 2018.

[45] S. Lophaven, H. Nielsen, J. Søndergaard, DACE - a Matlab Kriging Toolbox, Version 2.0, 2002.

[46] I. Sobol, Global sensitivity indices for nonlinear mathematical models and their Monte Carlo estimates, in: The Second IMACS Seminar on Monte Carlo Methods, Math. Comput. Simul. 55 (2001) 271–280, https://doi.org/10.1016/S0378-4754(00)00270-6.

[47] W. Hoeffding, A class of statistics with asymptotically normal distribution, Ann. Math. Stat. 19 (1948) 293–325, https://doi.org/10.1214/aoms/1177730196.

[48] T. Homma, A. Saltelli, Importance measures in global sensitivity analysis of nonlinear models, Reliab. Eng. Syst. Saf. 52 (1996) 1–17, https://doi.org/10.1016/0951-8320(96)00002-6.